Lateral load capacity of WikiHouse composite walls from CNC cut timber panels

Gabriele Granello[1], Thomas Reynolds[2], Rafik Taleb[3] and Clayton Prest [4]

ABSTRACT

Computer-numerical-control (CNC) fabrication of interlocking-plate timber structures is a novel construction method that allows to build structural elements without mechanical fasteners: the load transfer mainly relies on direct contact and friction between the composing panels. In this work, the lateral load capacity of shear walls formed from interlocking CNC cut plywood elements is investigated by means of experimental testing and analytical modelling. The experimental campaign comprises four full scale 5.4 m x 3.1 m wall specimens with and without window openings, and component tests on shear connectors and pegged connections which resist uplift at the base of the wall. The results obtained from the connection tests were used in combination with a proposed analytical model to simulate the force-displacement response of the full scale specimens. Results show that the behaviour of the walls is governed by the stiffness and capacity properties of the connectors. The elastic analytical model of the racking behaviour of the wall captured the stiffness of each of the specimens well once a global

[1]Engineering Lead, Open Systems Lab. Former Research Associate at the Institute for Infrastructure and Environment, School of Engineering, University of Edinburgh. e-mail:gabriele@opensystemslab.io

[2]Chancellor's Fellow, Institute for Infrastructure and Environment, School of Engineering, University of Edinburgh. e-mail: T.Reynolds@ed.ac.uk

[3]Research Associate, Institute for Infrastructure and Environment, School of Engineering, University of Edinburgh. e-mail: rtaleb@ed.ac.uk

[4]Research and Development Lead, Open System Lab. e-mail: clayton@opensystemslab.io

factor is applied to capture the effect of joint tolerance and other rigid body rotations, and the lateral load capacity of the walls fell within the range of predictions.

Keywords: Wikihouse, Digital fabrication, timber, plywood, carpentry

INTRODUCTION

Extensive research has been carried out in the space of off-site construction methods in the last few years, aiming to optimize the construction process in terms of time, cost and material use (Pan et al. 2008; Pan and Sidwell 2011; Arif et al. 2012; Boyd et al. 2013; Hosseini et al. 2018; Hairstans and Smith 2018; Duncheva and Bradley 2019).

In timber buildings, structural elements are usually fabricated in the factory and then assembled on site (Mayo 2015). Such a process can be further optimized within the same workflow, normally referred as design for assembly (Boothroyd 1987).

With the advent of digitisation and computer-numerical-control (CNC) machining, timber components can be digitally designed and fabricated to optimize the material use, as well as simplifying the assembly process (Beorkrem 2017; Nguyen et al. 2019).

Several research studies have explored the potential benefits of digital fabrication of timber structures. Magna et al. (2013) proposed a framework that combines finite element modelling with fabrication constraints, to optimize the design and fabrication of timber shell structures. Gattas and You (2016) proposed the concept of folded sandwich structures, achieving complex surfaces from a combination of simple shapes. Willmann et al. (2016) presented the current state of the art of robotic timber construction technologies. The authors showed that current setups, for example based on six-axis overhead gantry robots, can manufacture building elements up to 48 m length. Robeller and Von Haaren (2020) investigated a new construction system for shell structures made from door- and window cut-offs resulting from cross laminated timber (CLT) production lines.

One of the challenges in digitally fabricated structures is to provide an effective connection between the timber panels that doesn't rely on extensive manual labour. The most commonly adopted solution is known as "integral mechanical attachments" (Sass 2007), and consists of timber to timber connections without (or with few) additional fixings. This has the main advantage of reducing construction time (Robeller 2015).

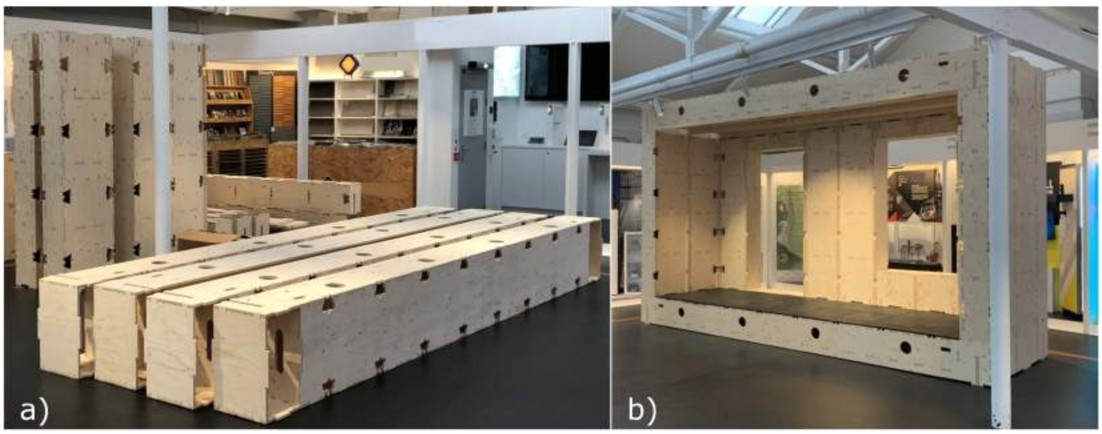

FIG. 1: Wikihouse Skylark installation at the Building Centre architectural gallery in London (UK): a) components and b) assembly. (Photo courtesy of Alastair Parvin)

The load carrying capacity of integral mechanical attachments was experimentally investigated by Rad et al. (2019). Three main parameters affecting the performance were identified: material type, timber fiber orientation, and tab insertion angle. Further tests were performed by (Gamerro et al. 2020), who concluded that the equations provided by Eurocode 5 (Comite Europeen de 2004) generally underestimates the load-carrying capacity of such connections by 25% (except when made from oriented strand board timber). Numerical models were also developed to simulate the joint behaviour, as proposed by Nguyen and Weinand (2018) and Stitic et al. (2019).

Integral mechanical attachments have been used in complete buildings. An early example is the "instant House" (Sass and Botha 2006), as well as the "Landesgartenschau Exhibition Hall" (Li and Knippers 2015) and the "Théâtre Vidy Lausanne" (Robeller et al. 2017).

An open-source building system based on digitally fabricated timber plates called *WikiHouse* started development in 2014. In 2022, a new WikiHouse system called *Skylark* (Granello et al. 2022) was developed with the goal of standardising the design, manufacturing, and assembly of low-rise residential buildings (Figure 1).

WikiHouse Skykark consists of structural elements (e.g. beams, columns, joints) manufactured by CNC machining 2.4 x 1.2 m plywood sheets, and assembled on site into walls and floors forming a modular structure.

In traditional timber construction, shear walls are made by plywood sheets are attached to the timber frame by mechanical fasteners, e.g., (Yasumura et al. 2006), or as 100-400 mm standalone mass plywood panels (Morrell et al. 2020). The behaviour of these systems has been extensively researched. However, a research gap currently exists regarding the lateral load behaviour of shear walls made by plywood elements using integral mechanical attachments, which transfer load in a fundamentally different way to these conventional systems.

The aim of this paper is to provide fundamental knowledge on this topic by investigating the lateral load response of complete CNC-cut shear wall systems with integral mechanical attachments. The scope of the work consists of an experimental campaign carried out on four full-scale wall specimens, four full-scale base connections and four full-scale shear connectors. An analytical model is then proposed to simulate the capacity of the walls.

All Skylark 3D models, CNC cutting related files and assembly instructions are available under Creative Commons Share-alike licence at www.wikihouse.cc. The 3D models, CNC cutting files, and assembly instructions for the specimens tested are provided as supplemental material to this paper.

EXPERIMENTAL TESTING

Full-scale walls

Four full scale wall specimens measuring 5.4m x 3.1 m x 0.3 m were tested in a under a racking load applied at a top corner. The specimens were fabricated from 2.4 m x 1.2 m x 18 mm plywood sheets using a 3 axis CNC machine (Figure 2).

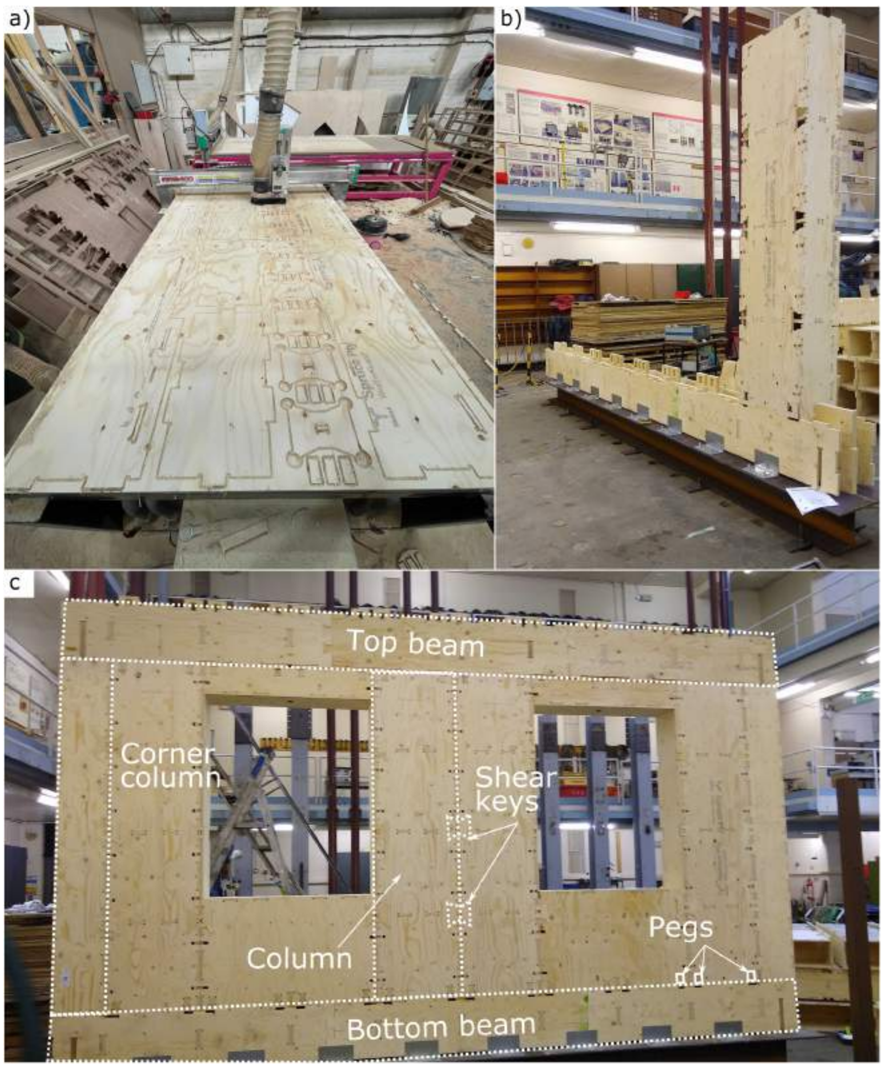

FIG. 2: Fabrication and assembly of the specimens: a) CNC cutting of the specimens, b) installation of the bottom beam and assembly of the first column, and c) final construction

Walls are made up of four different element types, and two connection types (Figure 2). The main elements composing the wall are: 1) top beam, 2) bottom beam, 3) corner column and 4) column. The connectors are : 1) shear key and 2) peg joint. The columns are connected to the top and bottom beams by using timber pegs of dimensions 264 mm x 60 mm x 18 mm running through the a shear panel. Furthermore, the columns are connected to each other (and to the corner columns) by using shear keys. More details on the geometry as well as the assembly sequence can be found in the 3D models and assembly guideline provided with this manuscript.

The plywood making up up the specimens is made up of four lamellae with grain oriented parallel to the longer direction of the panel (indicated with $||$), and two lamellae with grain oriented perpendicular to the longer direction of the panel (indicated with $\perp$). Its average material properties, which were obtained by means of experimental testing (Granello et al. 2022), are summarized in Table 1.

TABLE 1: Mechanical properties of plywood: σ_c compression capacity, E_c elastic modulus in compression, σ_t tension capacity, E_t elastic modulus in tension, f_s shear capacity and G shear modulus.

	direction $\|\|$	direction $\perp$
σ_c (MPa)	24.6	15.4
E_c (MPa)	9969	3549
σ_t (MPa)	18.5	15.2
E_t (MPa)	8532	4423
f_s (MPa)	5.4	*6.3
G (MPa)	183.9	*141.7

* No actual shear failure plane was identified.

The specimens comprise walls with and without 1.2 m^2 openings for windows. For each geometric configuration, two tests were carried out, one with and one without a constant distributed vertical load on the top beam. To distinguish more easily between the specimens, the following labels are used:

- SW_noLoad: the specimen is a solid wall (no windows), and no vertical load was applied during the test.

- SW_Load: the specimen is a solid wall, constant vertical load was applied during the test.
- WW_noLoad: the specimen has two 1.2 m^2 openings for windows, and no vertical load was applied during the test.
- WW_Load: the specimen has two 1.2 m^2 openings for windows, and costant vertical load was applied during the test.

The experimental setup used for the test can be seen in Figure 3. Specimens were bolted to a UC 305 mm x 305 mm x 188 mm S235 steel beam by using 8 pairs of L-shape aluminium steel plates. Each aluminium steel plate was connected to the timber specimen by using thirty-five 5 mm diameter screws. The aluminium plates were bolted to the steel beams by using two 8.8 M16 bolts. The specimen to steel foundation connection was designed with extra capacity to make sure that failure would occur in the timber specimen. The steel beam was connected to the laboratory strong floor by using twelve 24 mm diameter steel threaded bars and nuts.

In terms of data acquisition, the behaviour of the specimen was monitored by:

1. Four linear displacement transducers measuring any uplift occurring between the specimen and the steel beam.
2. two linear displacement transducers monitoring the diagonal displacements in correspondence of the central point of the specimen;
3. two string potentiometers to measure the horizontal displacement placed on the top corners or the specimen;
4. A load cell placed between the actuator and the specimen;

On the opposite side of the one visible in Figure 3, the specimen was painted white and marked with a series of approximately 1.5 cm diameter speckles. That allowed to track the motion of the specimen by using single-camera, two dimensional Digital

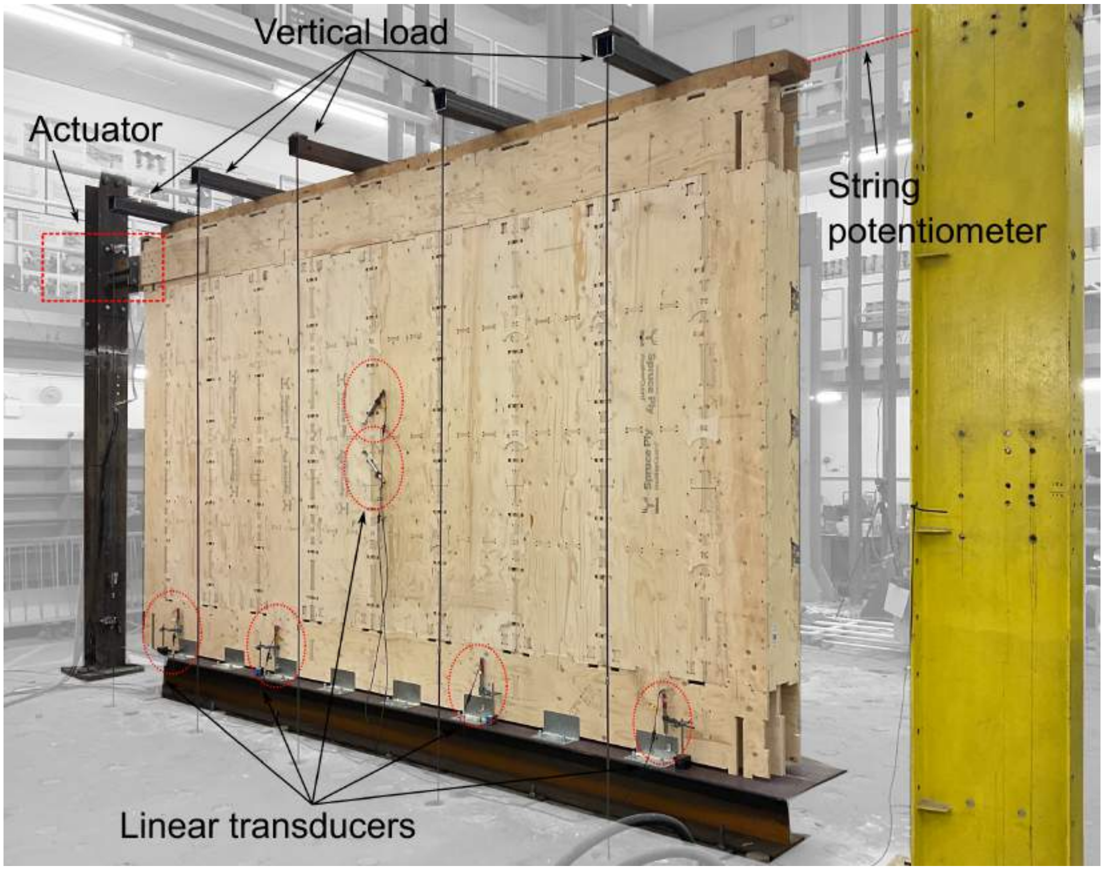

FIG. 3: Experimental setup for testing the walls.

Image Correlation (DIC).

When vertical load was present, it was applied to the specimen by using 5 C-shaped steel beams, which were connected to the actuators placed under the strong floor. The 5 beams had a distance of 1143 mm between each other, equivalent to a linear load of 8.3 kN/m. The linear load was chosen to represent the serviceability gravity load of a potential storey above the wall.

Out of plane restraint was provided at the top of the panel by two struts fixed to balcony of the laboratory. The connection between the struts and the specimen was designed to allow for relative sliding and rotation being developed during the in-plane motion.

The lateral load was applied at mid-height of the top beam using a hydraulic actuator (Figure 3). The loading protocol was design in accordance with the EN 594:2011 (2011), i.e.,:

1. cycle 1: load up to 10% of the estimated panel capacity, maintain for 30 seconds, and unload;
2. cycle 2: load up to 40% of the estimated panel capacity, maintain for 30 seconds, and unload;
3. cycle 3: load up to failure.

The panel capacity, based on preliminary tests on the connectors, was estimated to be 80 kN.

The force-displacement response of the specimens is reported in Figure 4. The displacement was taken in correspondence of the corner opposite to the point of application of the lateral force, the top right corner of the specimen in Figure 3. From Figure 4, it can be noticed the SW_noLoad failed at a peak force of 65 kN. The failure was caused by reaching the capacity of the pegs resisting the uplift of the wall at the same end as the actuator, i.e., the connection between the bottom beam and the columns as reported in Figure 5a,b.

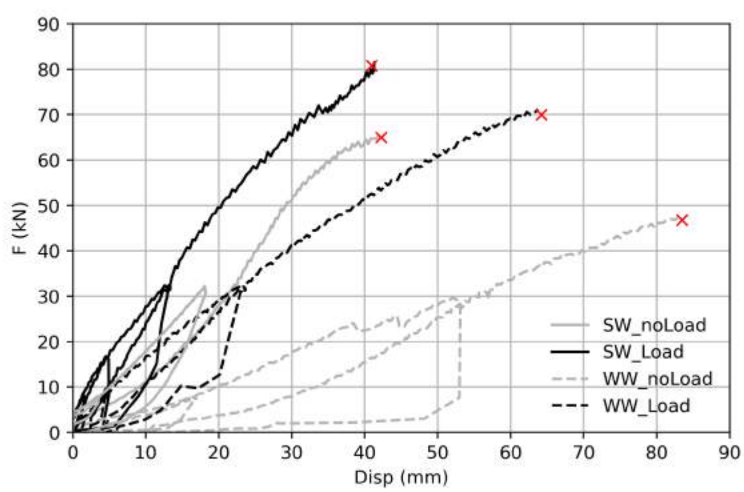

FIG. 4: Force-displacement response of the specimens.

The solid wall SW_Load reached a maximum capacity of 82 kN, i.e., 26% higher than without gravity loads. The specimen did not reach failure of any component. However, the test had to be stopped for safety reasons because the specimen was significantly leaning out of plane as reported in in Figure 5c.

The WW_noLoad specimen failed at a peak force of 47 kN. Inspection of the specimen revealed the failure of the pegs at the bottom left corner of the specimen (Figure 5d). There was also failure of a shear connection where a split had formed between the corner of the shear connector and the window opening, as reported in Figure 5e.

The WW_Load specimen failed at a peak force of 70 kN, i.e., 75% higher than the same geometry wall without vertical loading. The inspection of the specimen revealed that the failure was again due to the failing of the pegs, as well as the failure of the shear connector under the opening similar to what already observed in the WW_noLoad specimen. Furthermore, in this specimen a significant shear deformation was observed in the central line of shear connectors between the columns as reported in Figure 5f.

No measurable uplift displacement was recorded in any of the specimens by the linear transducers between the steel beam and the timber beam. The displacements recorded by the central linear transducers and the string potentiometers were used to verify the displacements measured by DIC, which will be discussed later.

Figure 4 shows the specimens do not follow the initial loading curve after they are unloaded. In fact, the specimens present a residual deformation when they are unloaded, and a shift is present in the re-loading branch with respect to the initial one. This effect is rather common in conventional timber connections with dowels or bolts, because the load is transferred by contact over a small area and local plastic deformation occurs even at low loads (Dorn et al. 2013; Reynolds et al. 2013). This effect is amplified in this system because of the several connections between panel to panel, and element to element, which all rely on timber to to timber load transfer.

FIG. 5: Failures observed in the specimens: a) b) pegs failure in the SW_noLoad specimen, c) out of plane bending in the SW_Load specimen, d) pegs failure and e) splitting in the WW_noLoad specimen, f) shear deformation in the WW_Load specimen.

The stiffness k_w of the panels was calculated according to equation 1.

$$k_w = \frac{F_{40\%} - F_{10\%}}{d_{40\%} - d_{10\%}} \tag{1}$$

$F_{40\%}, F_{10\%}$ represent 40% and 10% of the peak force, and $d_{40\%} - d_{10\%}$ represent 40% and 10% of the deformation at such level of force. To be consistent among the specimens, the stiffness was calculated on the second cycle of the loading-unloading protocol.

The highest stiffness, 2378 kN/m, was observed in the SW_Load specimen, while the specimen with similar geometry but without vertical load presented a stiffness values of 1639 kN/m. A stiffness of 1338 kN/m was calculated for the WW_Load specimen, while a stiffness of 638 kN/m was found for the WW_noLoad specimen. The addition of vertical load increased the stiffness by 45% in the solid wall case, and 110% in the wall with openings case. Results are summarized in Table 2.

TABLE 2: Experimental results: F_{max} peak load and k_w stiffness of the wall.

Specimen	**Window**	**Vertical load**	F_{max} **[kN]**	k_w **[kN/m]**
SW_noLoad	no	no	65	1639
SW_Load	no	yes	82	2378
WW_noLoad	yes	no	47	638.0
WW_Load	yes	yes	70	1338

The deformed shape at failure of specimens SW_noLoad and WW_noLoad was obtained by DIC, and is shown in Figure 6. Similar deformed shapes were observed for the other two cases. Note that the amount the displacements was increased by a factor of 20 to provide a better visualization.

From Figure 6, it can be noticed that both walls tend to pivot around the internal side of the right corner column, and the majority of displacement is accumulated in the gap between the the columns and the bottom beam. By observing the motion of the panel, two main contributions in terms of displacement can be observed:

1. A rigid body rotation with respect to the pivot point.
2. A shear deformation by which the columns slide vertically on each other.

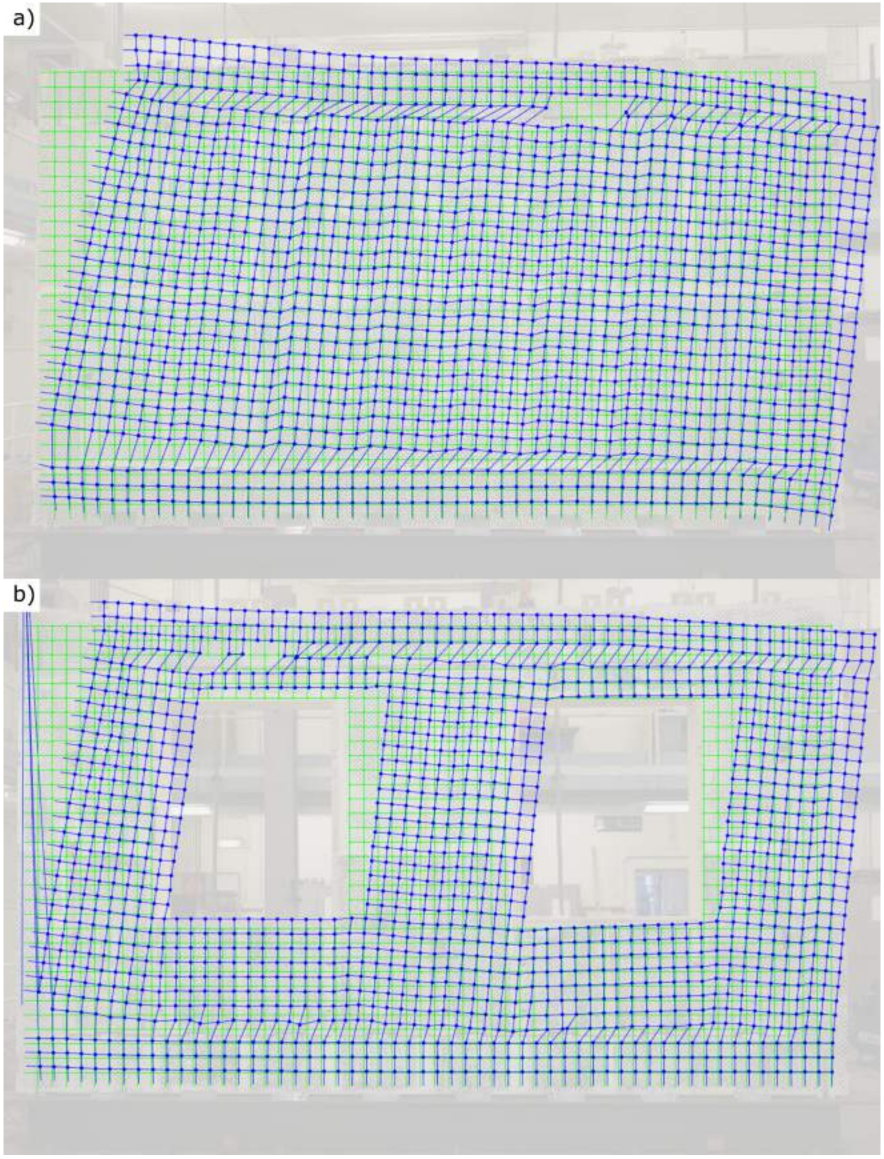

FIG. 6: Deformed shape at failure obtained by Digital Image Correlation for the a) SW_noLoad specimen and b) WW_noLoad specimen.

The top beam was observed to deform with a double-curvature profile, which is typical of beams in moment-resisting frames. Further details will be presented in a later section, where the problem is formalized as a simplified analytical model.

Shear keys

The shear behavior of the shear keys was tested separately to investigate its capacity and stiffness. A total of four specimens was tested in a shear setup made of three mock columns connected by four connectors (two per face), which were sheared off by using an hydraulic actuator (Figure 7). Below each of the shear keys, a potentiometer was placed to measure the displacement parallel to the shear plane.

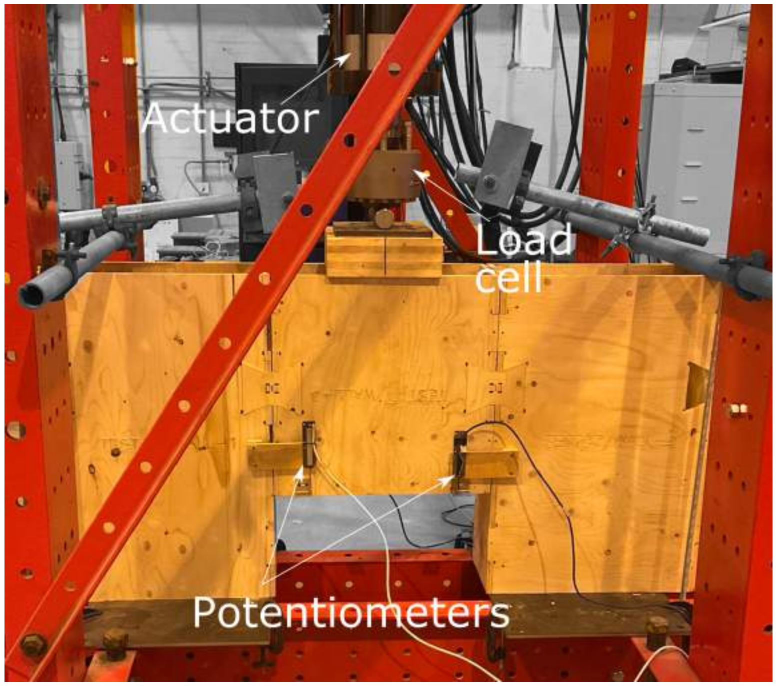

FIG. 7: Experimental setup to test the shear connectors.

Depending on how the shear keys are oriented on the plywood panel during fabrication, they may have either four or two lamellae parallel to the shear plane (Fig 8). To distinguish between the two cases, the following notation is used:

- $PLY \updownarrow$, to indicate the shear key with four lamellae with grain parallel to the shear plane.
- $PLY \leftrightarrow$, to indicate the shear key with two lamellae with grain parallel to the shear plane.

Two different loading protocols were used:

1. monotonic load, to identify the maximum connection capacity per shear plane.


a)

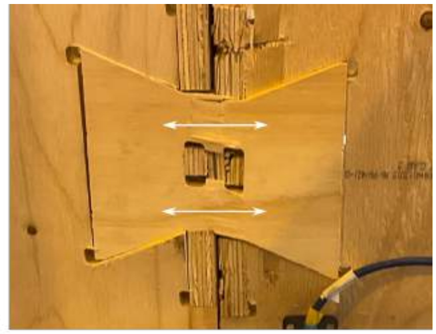
b)

FIG. 8: Two possible grain orientations: a) 4 lamellae with grain parallel to the shear plane, 2) 2 lamellae with grain perpendicular to the shear plane.

2. cyclic (load-unload-reload) protocol according to BS EN 26891-1991 (Comite Europeen de Normalisation 1991), to identify any difference between initial and unload-reload stiffness.

Experimental results in terms of force-displacement per shear plane are reported in Figure 9. Note that the force per shear plane is taken as half of the force measured at the actuator, while the displacement is taken as the average between the two potentiometers measuring opposite faces of the same shear plane.

Figure 9 shows that the peak force for the $PLY \updownarrow$ specimens was 11.2 kN using the monotonic loading protocol and 10.8 kN using the cylic protocol. The peak force for the $PLY \leftrightarrow$ specimens was 12.6 kN using the monotonic loading protocol and 13.5 kN using the cyclic protocol.

During the test, no damage was observed in the main elements: failure was only observed in the shear keys themselves. Pictures of the observed failure modes are reported in Figure 10.

Fig. 10 shows that the lamellae with grain parallel to the plane in the plywood specimens exhibit a clear shear failure. Conversely, the lamellae with grain perpendicular to the shear plane are subjected to what seems to be a tensile failure.

The deformed shape at failure of specimen $PLY \updownarrow$ tested with monotonic load is

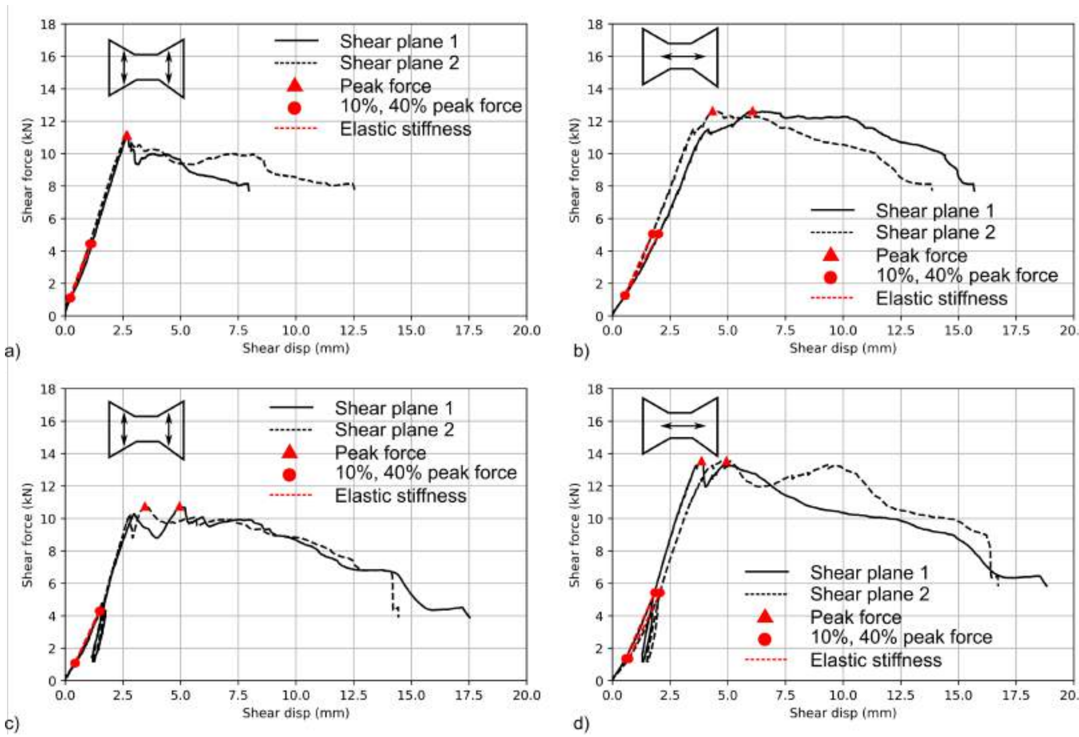

FIG. 9: Force-displacement experimental results obtained for each shear plane: a), c) monotonic and cyclic test on plywood specimens with 4 lamellae which grain is parallel to the shear plane; b), d) monotonic and cyclic test on plywood specimens with 2 lamellae in which the grain is parallel to the shear plane.

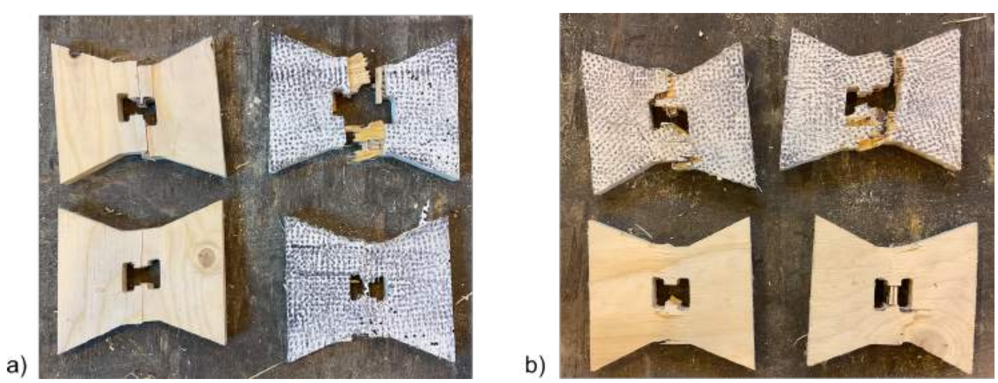

FIG. 10: Observed failure modes in the: a) $PLY \updownarrow$ specimens, b) $PLY \leftrightarrow$ specimens.

shown in Figure 11a. Note that the amount the displacements was increased by a factor of 10 to provide a better visualization.

The shear key element is subjected to a combination of shear deformation and tensile deformation. This is because the bow tie is forced to progressively rotate while the vertical displacement increases: the bow ties is in fact constrained to follow the displacements imposed by the surrounding blocks. The two deformation mechanisms are graphically represented in Figure 11b.

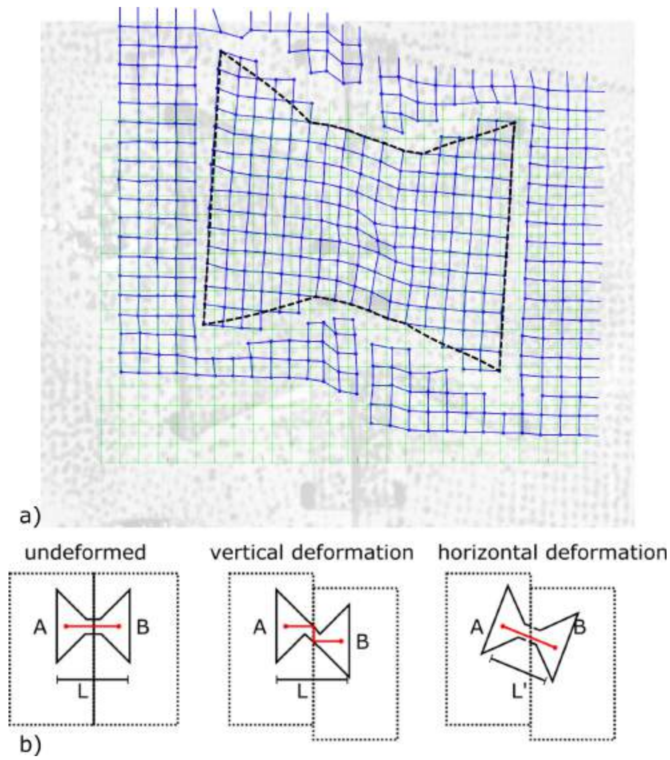

FIG. 11: Deformed shape of the shear keys: a) captured by using DIC analysis and b) conceptual behaviour.

The stiffness k_s of timber connections is calculated using equation 2:

$$k_s = \frac{F_{40\%} - F_{10\%}}{d_{40\%} - d_{10\%}} \tag{2}$$

where $F_{40\%}, F_{10\%}$ represent 40% and 10% of the maximum force (Fig. 9). $d_{40\%}, d_{10\%}$ represent the values of differential in-plane displacement where such force occurs.

The slip modulus k_s ranges between 5.3 kN/mm and 5.7 kN/mm for $PLY \updownarrow$, while it ranges between 6.0 kN/mm and 6.5 kN/mm for $PLY \updownarrow$. Therefore, orienting the connection having four lamellae perpendicular to the shear plane can provide slightly higher stiffness than having four lamellae parallel to the shear plane. This seems counter intuitive. However, this depends on the different deformation contributions given by the two mechanisms described in Figure 11b. If the main stiffness contribution comes from the tensile elongation of the specimen rather that the shear one, then having four lamellae with grain parallel to such elongation will provide higher stiffness. Given the fact the gaps exist between the bow tie and the surrounding, the second mechanism is believed to be more facilitated.

TABLE 3: Experimental values of the bow ties tested in shear: F_max; maximum force per shear plane (SP), $d_{10\%}$ differential shear displacement corresponding to 10% of the maximum force, $d_{40\%}$ differential shear displacement corresponding to 40% of the maximum force, k_s shear stiffness of the connection.}

Specimen	**Load type**	F_{max} **(kN)**	$d_{10\%}$ **(mm)**		$d_{40\%}$ **(mm)**		k_s **(kN/mm)**		
			SP1	**SP2**	**SP1**	**SP2**	**SP1**	**SP2**	**average**
$PLY \updownarrow$	monotonic	11.1	0.185	0.244	1.06	1.16	5.7	5.7	5.7
	cyclic	10.8	0.409	0.431	1.47	1.52	5.3	5.3	5.3
$PLY \leftrightarrow$	monotonic	12.6	0.523	0.567	1.73	2.01	6.1	5.9	6.0
	cyclic	13.5	0.71	0.523	2.07	1.83	6.4	6.5	6.5

Column to beam connection via pegs

The column to beam connection was tested separately to obtain experimental data regarding its capacity and stiffness. Four joint specimens, geometry slightly modified to allow for a compression test instead of a tension test for practical reasons, were tested in a compression setup (Figure 12). The setup was designed to replicate the same failure mode observed in the testing of the walls. The specimens comprise the following:

1. two plywood specimens, labelled $PLY \leftrightarrow$ where the timber pegs had four plies with the grain oriented perpendicular to the load direction.
2. two plywood specimens, labelled $PLY \updownarrow$ where the timber pegs had four plies with the grain oriented parallel to the load direction.

The joints were tested by using a monotonic displacement control loading protocol to estimate their capacity as well as by applying a load-unload-reload protocol according to the EN 1380:2009 (Comité Européen de Normalisation 2009).

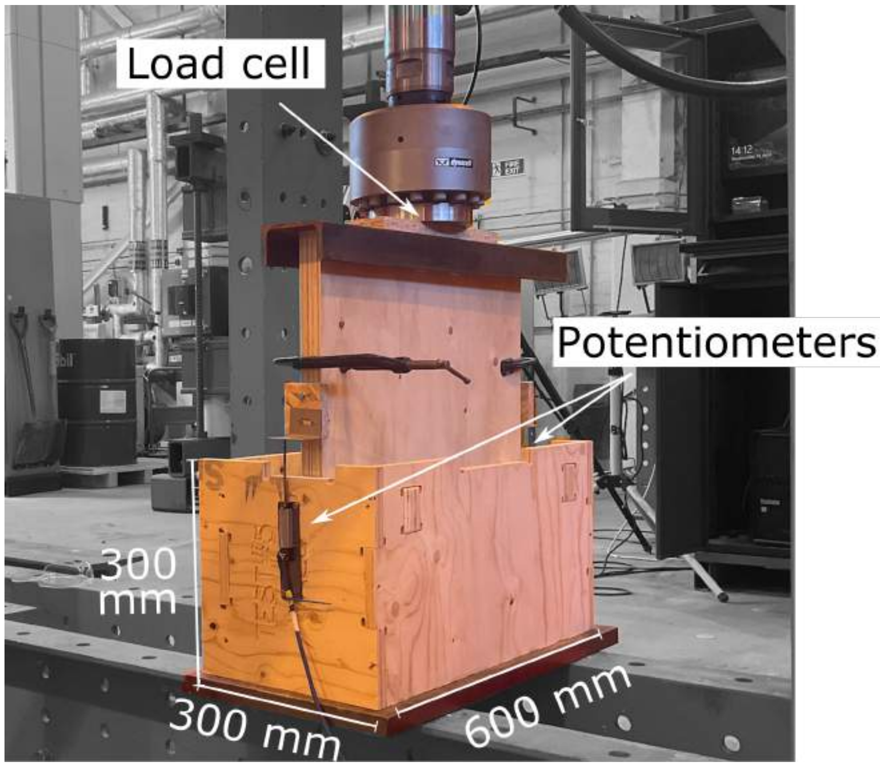

FIG. 12: Experimental setup to test the shear panel to column load path capacity (via pegs).

A load cell was placed between the actuator and the specimen to measure the applied load (Figure 12). Two linear potentiometers (one on each side) were installed on the specimen to measure the relative displacement between the shear panel and the mock column.

All specimens failed because of one of the pairs of pegs, as can be seen from Figure 13. No other damage was observed on the specimen while inspecting the different components of the joint, similarly to what observed in the full scale walls.

The force-displacement results of the test are reported in Figure 14 and Table 4.

From Figure 14 and Table 4, it can be noticed that the maximum upflifing capacity

FIG. 13: Observed failure mode.

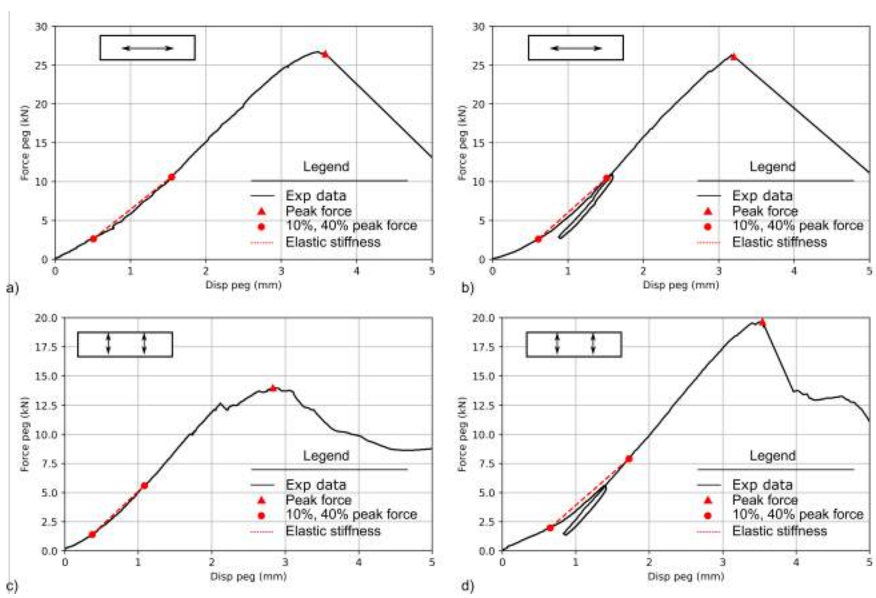

FIG. 14: Force-displacement experimental results of the column to beam connection via pegs.

TABLE 4: Experimental values of the column to beam connection due to uplifting forces: F_{max}; maximum force, $d_{10\%}$ displacement corresponding to 10% of the maximum force, $d_{40\%}$ displacement corresponding to 40% of the maximum force, k_u elastic stiffness of the connection.}

Specimen	**Load type**	F_{max} **(kN)**	$d_{10\%}$ **(mm)**	$d_{40\%}$ **(mm)**	k_u **(kN/mm)**
$PLY \leftrightarrow$	monotonic	26.5	0.51	1.6	7.6
	cyclic	26.1	0.37	1.5	8.6
$PLY \updownarrow$	monotonic	14.0	0.36	1.1	5.9
	cyclic	19.7	0.65	1.7	5.5

for the joint is equal to 26.5 kN for the $PLY \leftrightarrow$ monotonic test, and 26.1 kN for the cyclic test. Concerning the $PLY \updownarrow$ specimen, the maximum uplifting capacity is equal to 14.0 kN for monotonic test, and 19.7 kN for the cyclic test. The joint uplifting stiffness k_u was calculated by applying equation 2; results are reported in Table 4. The elastic stiffness, k_u was found to be equal to 7.6 kN/m and 8.6 kN/m for the $PLY \leftrightarrow$ specimen when using the monotonic and cyclic protocol, respectively. k_u was found to be equal to 5.9 kN/m and 5.5 kN/m for the $PLY \updownarrow$ specimen when using the monotonic and cyclic protocol, respectively.

ANALYTICAL MODEL

Model formulation

An analytical model is proposed to simulate the response of the walls (Figure 15). The aim is to capture lateral force vs horizontal displacements of the walls, as well as the vertical displacement profile observed by using DIC (Figure 6).

The formulation of the problem comprises three parts:

1. global equilibrium: the sum of moments generated by the external forces with respect to the pivoting point is equal to zero;
2. local equilibrium: the sum of the vertical forces in each column is equal to zero;

3. elastic constitutive law: the shear force in the bow ties and the uplifting force in the pegs are directly proportional to their displacement and stiffness.

For sake of simplification, the contribution of the top beam is neglected.

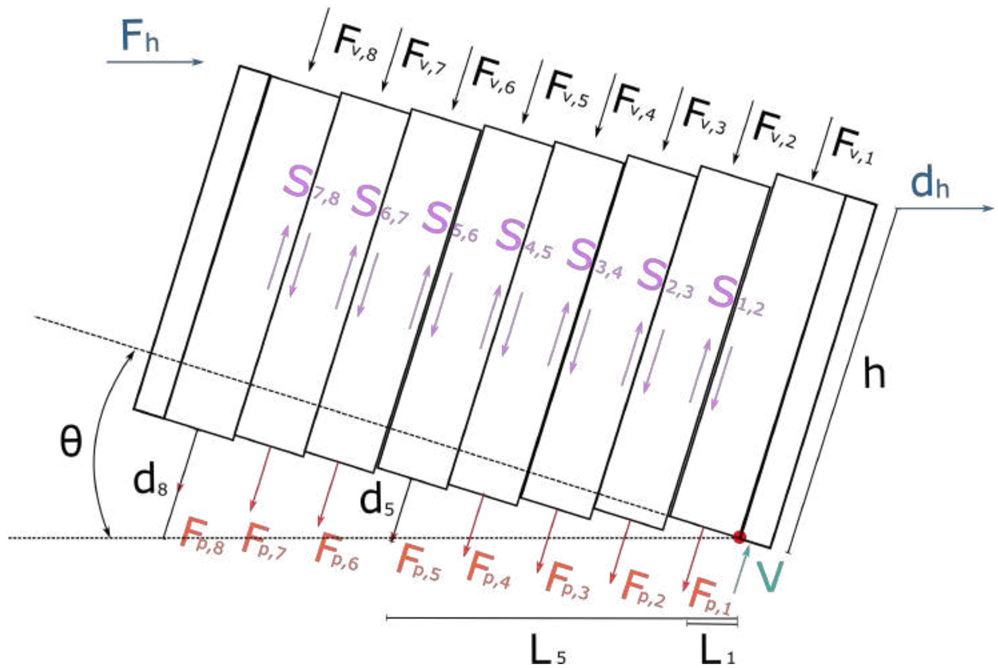

FIG. 15: Analytical model of the wall.

By labelling with F_h the external horizontal, $F_{v,i}$ the vertical forces acting on each column, $F_{p,i}$ the force exerted by the pegs, h the distance between the point of application of F_h to the pivoting point and L_i the distance between each peg to the pivoting point, the equilibrium of the moments can be written according to equation 3.

$$\sum_{i=1}^{8} F_{p,i} L_i - F_h h = -\sum_{i=1}^{8} F_{v,i} L_i \tag{3}$$

For each column the vertical equilibrium is imposed by eq. 4.

$$\begin{cases} i = 1 & -F_{p,1} + V - S_{1,2} = F_{v,1} \\ i \neq 1,8 & -F_{p,i} + S_{i-1,i} - S_{i,i+1} = F_{v,i} \\ i = 8 & -F_{p,8} + S_{7,8} = F_{v,8} \end{cases} \tag{4}$$

with V the vertical reaction arising near the pivoting point, and $S_{i,i+1}$ the shear contact forces between column i and column $i+1$.

The generic force on the i^{th} peg due to a given rotation θ imposed to the wall is expressed by eq. 5.

$$\begin{cases} i = 1 & F_{p,1} = \theta L_1 k_u \\ i \neq 1 & F_{p,i} = \theta L_i k_u - \sum_{j=1}^{i} \frac{k_u}{k_{j-1,j}} S_{j-1,j} \end{cases} \tag{5}$$

with k_u the stiffness of the pegs due to uplifting, and $k_{j-1,j}$ the shear stiffness between the column $j-1$ and j. While k_u is expected to be the same for all the columns, $k_{j-1,j}$ depends on the number of shear keys at the interface.

Equations 3, 4 and 5 are combined into a linear system (eq. 6), so that it can be solved for a specific value of θ:

$$\begin{bmatrix}
L_1 & 0 & L_2 & 0 & L_3 & 0 & L_4 & 0 & L_5 & 0 & L_6 & 0 & L_7 & 0 & L_8 & -h & 0 \\
-1 & -1 & 0 & 0 & 0 & 0 & 0 & 0 & 0 & 0 & 0 & 0 & 0 & 0 & 0 & 0 & 1 \\
0 & 1 & -1 & -1 & 0 & 0 & 0 & 0 & 0 & 0 & 0 & 0 & 0 & 0 & 0 & 0 & 0 \\
0 & 0 & 0 & 1 & -1 & -1 & 0 & 0 & 0 & 0 & 0 & 0 & 0 & 0 & 0 & 0 & 0 \\
0 & 0 & 0 & 0 & 0 & 1 & -1 & -1 & 0 & 0 & 0 & 0 & 0 & 0 & 0 & 0 & 0 \\
0 & 0 & 0 & 0 & 0 & 0 & 0 & 1 & -1 & -1 & 0 & 0 & 0 & 0 & 0 & 0 & 0 \\
0 & 0 & 0 & 0 & 0 & 0 & 0 & 0 & 0 & 1 & -1 & -1 & 0 & 0 & 0 & 0 & 0 \\
0 & 0 & 0 & 0 & 0 & 0 & 0 & 0 & 0 & 0 & 0 & 1 & -1 & -1 & 0 & 0 & 0 \\
0 & 0 & 0 & 0 & 0 & 0 & 0 & 0 & 0 & 0 & 0 & 0 & 0 & 1 & -1 & 0 & 0 \\
1 & 0 & 0 & 0 & 0 & 0 & 0 & 0 & 0 & 0 & 0 & 0 & 0 & 0 & 0 & 0 & 0 \\
0 & \frac{k_u}{k_{1,2}} & 1 & 0 & 0 & 0 & 0 & 0 & 0 & 0 & 0 & 0 & 0 & 0 & 0 & 0 & 0 \\
0 & \frac{k_u}{k_{1,2}} & 0 & \frac{k_u}{k_{2,3}} & 1 & 0 & 0 & 0 & 0 & 0 & 0 & 0 & 0 & 0 & 0 & 0 & 0 \\
0 & \frac{k_u}{k_{1,2}} & 0 & \frac{k_u}{k_{2,3}} & 0 & \frac{k_u}{k_{3,4}} & 1 & 0 & 0 & 0 & 0 & 0 & 0 & 0 & 0 & 0 & 0 \\
0 & \frac{k_u}{k_{1,2}} & 0 & \frac{k_u}{k_{2,3}} & 0 & \frac{k_u}{k_{3,4}} & 0 & \frac{k_u}{k_{4,5}} & 1 & 0 & 0 & 0 & 0 & 0 & 0 & 0 & 0 \\
0 & \frac{k_u}{k_{1,2}} & 0 & \frac{k_u}{k_{2,3}} & 0 & \frac{k_u}{k_{3,4}} & 0 & \frac{k_u}{k_{4,5}} & 0 & \frac{k_u}{k_{5,6}} & 1 & 0 & 0 & 0 & 0 & 0 & 0 \\
0 & \frac{k_u}{k_{1,2}} & 0 & \frac{k_u}{k_{2,3}} & 0 & \frac{k_u}{k_{3,4}} & 0 & \frac{k_u}{k_{4,5}} & 0 & \frac{k_u}{k_{5,6}} & 0 & \frac{k_u}{k_{6,7}} & 1 & 0 & 0 & 0 & 0 \\
0 & \frac{k_u}{k_{1,2}} & 0 & \frac{k_u}{k_{2,3}} & 0 & \frac{k_u}{k_{3,4}} & 0 & \frac{k_u}{k_{4,5}} & 0 & \frac{k_u}{k_{5,6}} & 0 & \frac{k_u}{k_{6,7}} & 0 & \frac{k_u}{k_{7,8}} & 1 & 0 & 0
\end{bmatrix}
\begin{bmatrix}
F_{p,1} \\ S_{1,2} \\ F_{p,2} \\ S_{2,3} \\ F_{p,3} \\ S_{3,4} \\ F_{p,4} \\ S_{4,5} \\ F_{p,5} \\ S_{5,6} \\ F_{p,6} \\ S_{6,7} \\ F_{p,7} \\ S_{7,8} \\ F_{p,8} \\ F_h \\ V
\end{bmatrix}
=
\begin{bmatrix}
-\sum_{i=1}^{8} F_{v,i} L_i \\ F_{v,1} \\ F_{v,2} \\ F_{v,3} \\ F_{v,4} \\ F_{v,5} \\ F_{v,6} \\ F_{v,7} \\ F_{v,8} \\ k_u L_1 \theta \\ k_u L_2 \theta \\ k_u L_3 \theta \\ k_u L_4 \theta \\ k_u L_5 \theta \\ k_u L_6 \theta \\ k_u L_7 \theta \\ k_u L_8 \theta
\end{bmatrix} \tag{6}$$

Once the horizontal force F_h is calculated, the lateral displacement d_h can be calculated according to equation 7:

$$d_h = \underbrace{\theta h}_{rigid\ rotation} + \underbrace{\frac{F_h h}{A_s G}}_{shear\ deformation} + \underbrace{\frac{F_h h}{2EI}}_{bending\ deformation} \tag{7}$$

with A_s the shear area of the wall, I the second moment of inertia, E and G the elastic modulus and shear modulus of the material, respectively.

Comparison with experimental results

The model was applied to simulate the response of the walls. The input parameters are summarized in Table 5.

The values of G, k_s and k_u obtained by means of experimental testing and reported in Table 1, 3 and 4. respectively. Since for the experimental campaign on the walls

TABLE 5: Parameters used in the analytical model: $F_{v,i}$ vertical force on the ith column, $k_{i,i+1}$ shear stiffness between the ith and i+1thcolumn and calibration factor.

Specimen	$F_{v,i}$ (kN) $i = 1,4,5,8$	$F_{v,i}$ (kN) $i = 2,3,6,7$	$k_{4,5}$ (kN/mm)	$k_{i,i+1}$ (kN/mm) $i \neq 4$
SW_noLoad	0.5	0.5	$3k_s$	$3k_s$
SW_Load	6.1	6.1	$3k_s$	$3k_s$
WW_noLoad	11.9	0.17	$3k_s$	k_s
WW_Load	11.9	0.17	$3k_s$	k_s

the connectors were fabricated with either grain orientations, the average values of $k_s = 5.9$ kN/mm and $k_u = 6.9$ kN/mm were used. The shear area of wall A_s is taken equal to $\frac{2}{3}$ of the total area of the wall, i.e., 193824 mm^2, and the second moment of inertia I is equal to 7.57e11 mm^4.

The response of the model in terms of lateral force vs horizontal displacement is compared with the experimental results in Figure 16.

Results show that the model is stiffer that the experimental results. This is believed due to two main reasons:

1. First, the proposed model is based on a constant value of elastic initial stiffness, which is in reality observed to be degrading in the tests.
2. Second, the fact that the columns are made by several panels connected together (which present some gaps in the connections due to manufacturing tolerances) increases the overall flexibility of the elements.

The same effect was also observed in a previous work focused on bending of CNC-cut timber beams with integral mechanical attachments (Granello et al. 2022), where the effective inertia of the elements was found to be in the range of 0.5-0.6 smaller than the elastic rigid one.

To take into account this effect at macro-scale level, a ”calibration factor” equal to 0.4 is applied to k_u and k_s. It can noticed from Figure 16 that the introduction of such coefficient provides a better match between the model and the experimental results.

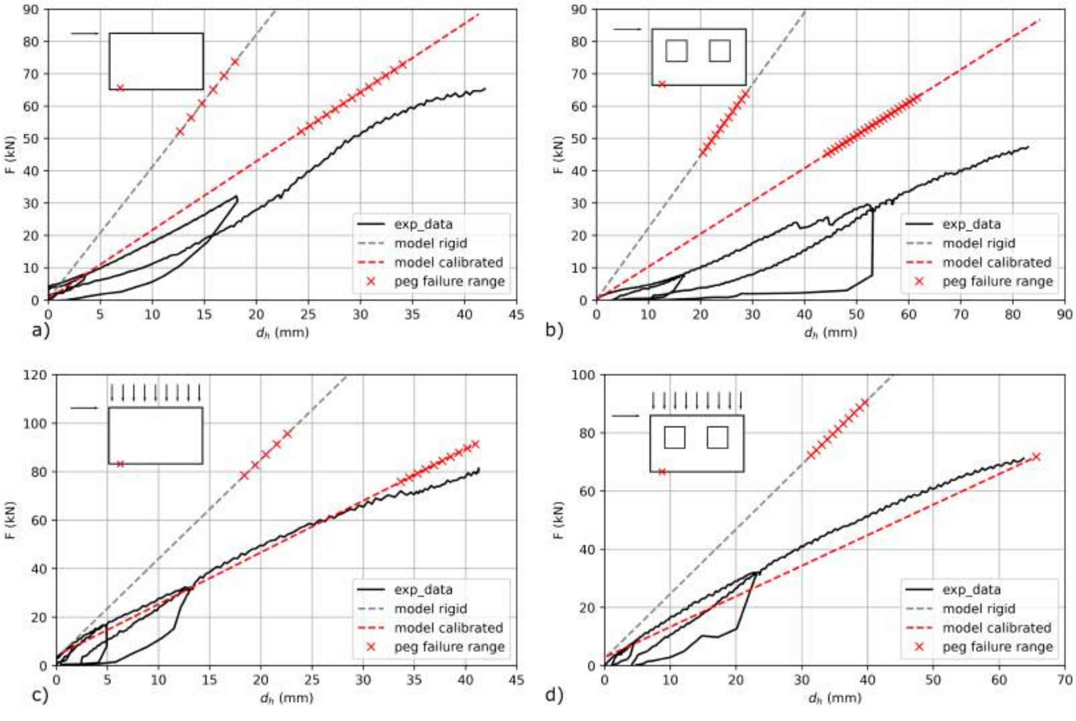

FIG. 16: Analytical model vs experimental results.

TABLE 6: Experimental vs modelling results.

Specimen	$F_{f,exp}(kN)$	$F_{f,model}(kN)$
SW_noLoad	65	52.1-73.2
SW_Load	> 82	78.6-95.6
WW_noLoad	47	45.2-63.8
WW_Load	70	72.2-89.6

The failure criteria in the model is based on what was observed experimentally, i.e.,the failure of the column to beam connection furthest from the rocking point. In the full scale experiment, pegs were oriented with their lamellae perpendicular to the main axis, hence the failure load varies between 14.0 kN and 19.7 kN (see Table 4).

By using this values, the minimum and maximum capacity of the walls are reported in Figure 16 and table 6. Results appear to be in agreement with the experimental values, within the range -20% to +36%.

The total force to be transferred in shear between the adjacent column sometimes exceeds the capacity of the shear connectors, however this force is not transferred by the shear connectors alone. The top beam will also restrain this movement, and some friction would also be generated between adjacent columns. The resistance to the shear force S in Figure 15 is therefore made up of all these mechanisms.

In Figure 17, the vertical displacements calculated with the model at peak load are compared with the ones measure by DIC.

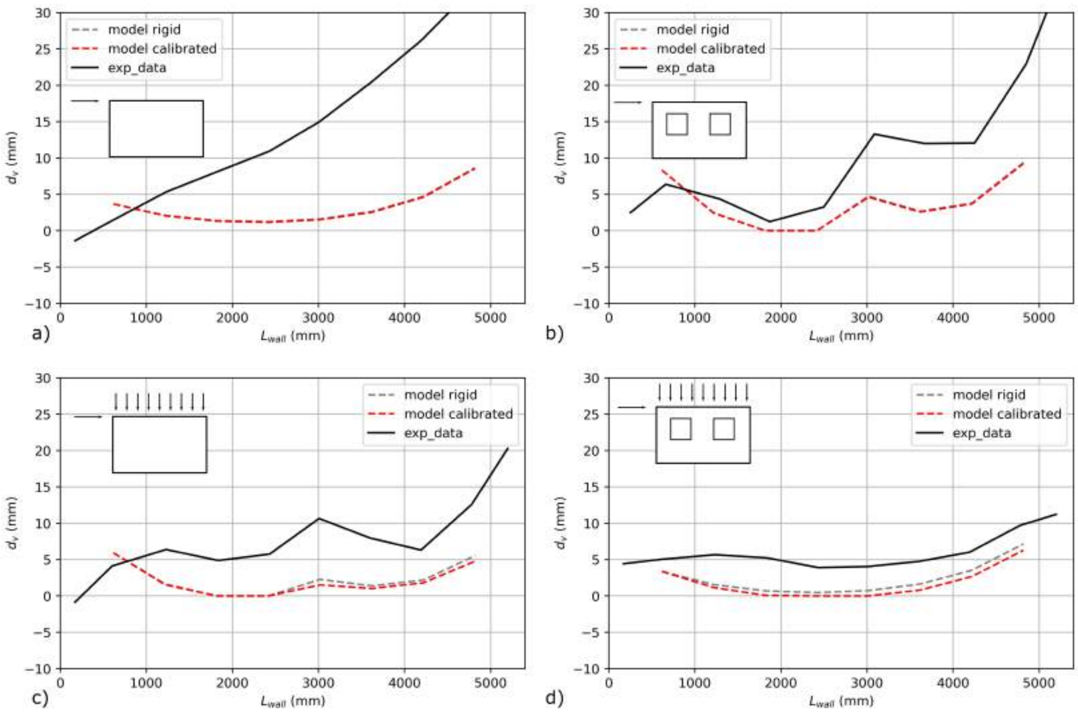

FIG. 17: Analytical model vs experimental results.

It can be noticed that, even if model can capture the shape of the vertical displacement profile in the gap opening, it underestimates the actual values when compared to the experimental results. Similarly to what stated before, this is believed due to the fact that treating the elements as rigid is too conservative. It can also be noticed that adopting an overall calibration factor does not improve the results. If greater accuracy is desired, most likely more complex numerical models e.g., (Nguyen and Weinand

2018; Stitic et al. 2019) are necessary.

CONCLUSION

The lateral load capacity of CNC timber panel WikiHouse walls was investigated by means of full scale experimental testing, connection testing and analytical modelling. The main findings of the study can be summarized as:

1. The lateral load capacity of the walls was found to be between 47 kN (wall with openings and without vertical load) and 82 kN (solid wall with vertical load).
2. The lateral stiffness of the walls was found to be between 638 kN/m (wall with openings and without vertical load) and 2370 kN/m (solid wall with vertical load).
3. The main failure mode was observed to be the rupture of an internal connection between the bottom part of the wall and the timber beam.
4. The DIC analysis revealed that the motion is a combination of rocking with respect to most external column, as well as shear deformation occurring in the columns and between the columns.
5. The proposed analytical model, which takes into account rocking and shear flexibility, was found stiffer than the experimental results. While the its response in terms of lateral force vs horizontal displacement can be calibrated by using a global calibration coefficient, it still underestimates the vertical displacements of the wall.
6. The proposed analytical model is capable of capturing capacity of the walls within a -20% to 30% accuracy range. However, uncertainty still exist in adequately capturing the shear force transfer between the columns.

More refined non linear models that can include friction between the columns and the contribution of the top beam are recommended to improve the accuracy of predictions, however the analytical model presented here is likely to be more appropriate for design offices.

ACKNOWLEDGEMENTS

The authors would like to thank Paul Rutherford from Threecreate for manufacturing and assembling the timber specimens. The help of technicians Mark Partington, Jim Hutcheson and Calum Melrose during the testing of the connections at the structural lab in Edinburgh University is greatly appreciated. Furthermore, the authors would like to thank Dave Brook from BRE for his great contribution in testing the full scale walls. The project was funded by Innovate UK, grant ID 77804.

REFERENCES

Arif, M., Goulding, J., and Rahimian, F. P. (2012). “Promoting off-site construction: Future challenges and opportunities.” *Journal of Architectural Engineering*, 18(2), 75–78.

Beorkrem, C. (2017). *Material strategies in digital fabrication*. Routledge.

Boothroyd, G. (1987). “Design for assembly—the key to design for manufacture.” *The International Journal of Advanced Manufacturing Technology*, 2(3), 3–11.

Boyd, N., Khalfan, M. M., and Maqsood, T. (2013). “Off-site construction of apartment buildings.” *Journal of architectural engineering*, 19(1), 51–57.

Comite Europeen de, N. (2004). *Eurocode 5 - Design of Timber Structures. Part1-1: General rules and rules for buildings*. Brussels, Belgium.

Comite Europeen de Normalisation (1991). *BS EN26891:1991 5 Timber structures - Joints made with mechanical fasteners - General principles for the determination of strength and deformation characteristics*. Brussels, Belgium.

Comite Europeen de Normalisation (2011). *EN 594:2011 - Timber structures - Test methods - Racking strength and stiffness of timber frame wall panels*. Brussels, Belgium.

Comité Européen de Normalisation (2009). “BS EN 1380:2009 Timber structures. Test methods. Load bearing nails, screws, dowels and bolts.

Dorn, M., de Borst, K., and Eberhardsteiner, J. (2013). “Experiments on dowel-type timber connections.” *Engineering structures*, 47(0), 67–80.

Duncheva, T. and Bradley, F. F. (2019). “Multifaceted productivity comparison of off-site timber manufacturing strategies in mainland europe and the united kingdom.” *Journal of Construction Engineering and Management*, 145(8), 04019043.

Gamerro, J., Bocquet, J. F., and Weinand, Y. (2020). “Experimental investigations on the load-carrying capacity of digitally produced wood-wood connections.” *Engineering Structures*, 213, 110576.

Gattas, J. and You, Z. (2016). "Design and digital fabrication of folded sandwich structures." *Automation in Construction*, 63, 79–87.

Granello, G., Reynolds, T., and Prest, C. (2022). "Structural performance of composite wikihouse beams from cnc-cut timber panels." *Engineering Structures*, 252.

Hairstans, R. and Smith, R. E. (2018). "Offsite hub (scotland): establishing a collaborative regional framework for knowledge exchange in the uk." *Architectural Engineering and Design Management*, 14(1-2), 60–77.

Hosseini, M. R., Martek, I., Zavadskas, E. K., Aibinu, A. A., Arashpour, M., and Chileshe, N. (2018). "Critical evaluation of off-site construction research: A scientometric analysis." *Automation in Construction*, 87, 235–247.

Li, J.-M. and Knippers, J. (2015). "Segmental timber plate shell for the landesgartenschau exhibition hall in schwäbisch gmünd—the application of finger joints in plate structures." *International Journal of Space Structures*, 30(2), 123–139.

Magna, R. L., Gabler, M., Reichert, S., Schwinn, T., Waimer, F., Menges, A., and Knippers, J. (2013). "From nature to fabrication: biomimetic design principles for the production of complex spatial structures." *International Journal of Space Structures*, 28(1), 27–39.

Mayo, J. (2015). *Solid wood: case studies in mass timber architecture, technology and design*. Routledge.

Morrell, I., Soti, R., Miyamoto, B., and Sinha, A. (2020). "Experimental investigation of base conditions affecting seismic performance of mass plywood panel shear walls." *Journal of Structural Engineering*, 146(8), 04020149.

Nguyen, A. C., Vestartas, P., and Weinand, Y. (2019). "Design framework for the structural analysis of free-form timber plate structures using wood-wood connections." *Automation in Construction*, 107, 102948.

Nguyen, A. C. and Weinand, Y. (2018). "Development of a spring model for the structural analysis of a double-layered timber plate structure with through-tenon joints."

World Conference of Timber Engineering 2018, number CONF, World Conference of Timber Engineering.

Pan, W., Gibb, A. G., and Dainty, A. R. (2008). “Leading uk housebuilders’ utilization of offsite construction methods.” *Building Research & Information*, 36(1), 56–67.

Pan, W. and Sidwell, R. (2011). “Demystifying the cost barriers to offsite construction in the uk.” *Construction Management and Economics*, 29(11), 1081–1099.

Rad, A. R., Weinand, Y., and Burton, H. (2019). “Experimental push-out investigation on the in-plane force-deformation behavior of integrally-attached timber through-tenon joints.” *Construction and Building Materials*, 215, 925–940.

Reynolds, T., Harris, R., and Chang, W.-S. (2013). “Viscoelastic embedment behaviour of dowels and screws in timber under in-service vibration.” *European Journal of Wood and Wood Products*, 71(5), 623–634.

Robeller, C. (2015). “Integral mechanical attachment for timber folded plate structures.” *Report no.*, EPFL.

Robeller, C., Gamerro, J., and Weinand, Y. (2017). “Théâtre vidy lausanne–a double-layered timber folded plate structure.” *Journal of the International Association for Shell and Spatial Structures*, 58(4), 295–314.

Robeller, C. and Von Haaren, N. (2020). “Recycleshell: Wood-only shell structures made from cross-laminated timber (clt) production waste.” *Journal of the International Association for Shell and Spatial Structures*, 61(2), 125–139.

Sass, L. (2007). “Synthesis of design production with integrated digital fabrication.” *Automation in construction*, 16(3), 298–310.

Sass, L. and Botha, M. (2006). “The instant house: a model of design production with digital fabrication.” *International Journal of Architectural Computing*, 4(4), 109–123.

Stitic, A., Nguyen, A. C., Rezaei Rad, A., and Weinand, Y. (2019). “Numerical simulation of the semi-rigid behaviour of integrally attached timber folded surface structures." *Buildings*, 9(2), 55.

Willmann, J., Knauss, M., Bonwetsch, T., Apolinarska, A. A., Gramazio, F., and Kohler, M. (2016). "Robotic timber construction—expanding additive fabrication to new dimensions." *Automation in construction*, 61, 16–23.

Yasumura, M., Kamada, T., Imura, Y., Uesugi, M., and Daudeville, L. (2006). "Pseudodynamic tests and earthquake response analysis of timber structures ii: two-level conventional wooden structures with plywood sheathed shear walls." *Journal of wood science*, 52(1), 69–74.